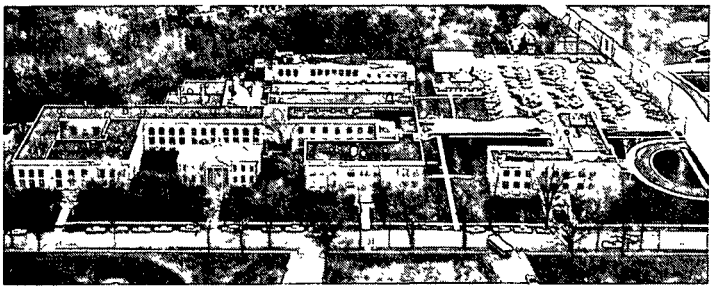

THE INSTITUTE OF PAPER CHEMISTRY, APPLETON, WISCONSIN

IPC TECHNICAL PAPER SERIES
NUMBER 293

# MODELING HEADBOX PERFORMANCE WITH COMPUTATIONAL FLUID MECHANICS

GARY L. JONES AND ROBERT J. GINNOW

JUNE, 1988

# Modeling Headbox Performance with Computational Fluid Mechanics

Gary L. Jones and Robert J. Ginnow

Portions of this work were used by RJG as partial fulfillment of the requirements for the Master of Science degree at The Institute of Paper Chemistry. This is to be presented at the TAPPI Engineering Conference in Chicago on September 19-22, 1988

# MODELING HEADBOX PERFORMANCE WITH COMPUTATIONAL FLUID MECHANICS

Gary L. Jones
Associate Professor
The Institute of Paper Chemistry
Appleton, WI 54912
U.S.A.

Robert J. Ginnow
Research Engineer
James River Corporation
Neenah, WI 54956
U.S.A.

## ABSTRACT

Until recently headbox design has been based exclusively on trial-and-error experimentation. Relative performance has been based on improved formation and sheet properties. Accurate numerical prediction of headbox flow could provide a more rapid and effective guide to improved headbox design.

A computational fluid mechanics program (FLUENT)™ (1) employing a finite difference numerical procedure and a k-ε turbulence model was used to predict turbulent flow profiles in several types of flow regimes: an experimental Conver-flo™ headbox, an experimental straight-channel diffuser and a free jet issuing from a hypothetical headbox.

In all cases, the velocity distributions were accurately predicted. Characteristics of the turbulent flow were also predicted with reasonable accuracy. Detailed turbulence intensity profiles revealed features not available experimentally. Jet shape predicted by FLUENT also agreed with irrotational flow theory.

Assumptions of uniform grid spacing, 2-dimensional analysis, uniform C-D profile, and isotropic turbulence may have limited the accuracy of the turbulence characteristics. While further work is suggested to improve the model, the procedure is successful and can be used to evaluate headbox design in terms of microturbulence generation.

## INTRODUCTION

The function of the headbox is to deliver a jet of fibrous stock uniformly across a moving wire to form paper (2). A second important function is to provide high intensity small scale turbulence to help disperse flocs and improve sheet formation (3). The headbox also levels out cross-currents and consistency variations and machine direction velocity gradients. It is also essential that the headbox alignment provide a jet which impinges on the wire at the correct location and angle.

Turbulence may be produced by a variety of elements such as perforated plates, rolls or screens. As the turbulent jet issues from the orifice, it expands into a region of more quiescent fluid, creating shear patterns, recirculating zones, and dissipating kinetic energy in the form of velocity fluctuations. Turbulent kinetic energy resulting from these velocity fluctuations tends to decrease, and eddy scales tend to increase downstream of the generating device.

FLUENT is a trademark of Creare, Inc. Conver-flo is a trademark of the Beloit Corporation.

Several studies (4,5,6) have attempted to measure pulp slurry turbulence exiting a headbox so that an effective microturbulence generator could be found through trial-and-error testing. Laser Doppler Anemometry (LDA) has proved successful in measuring turbulence intensity and scale. Through LDA, Chuang (5) found that turbulence level near the headbox exit is inversely related to consistency, converging angle and jet speed. Eddy size was directly related to hydraulic diameter, with small eddies decaying faster than larger eddies. High speed photographs showed that floc size was qualitatively correlated with turbulence eddy size.

The jet emerging from a headbox slice contracts in thickness and deflects downward as a result of slice geometry and gravity. Equations derived from conformal mapping of irrotational flows developed by Appel and Yu (7) predict both the angle and contraction of the jet as shown in Fig. 1. Graphs developed from these equations by TAPPI may be found in the TAPPI Technical Information Sheets (8).

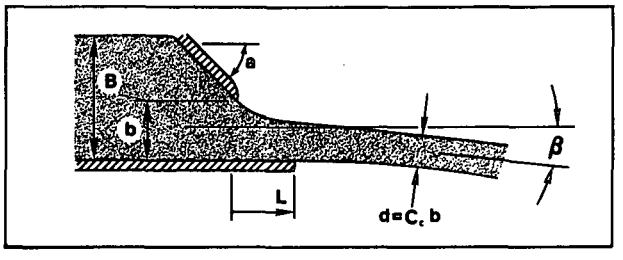


**Fig. 1** A typical headbox jet showing deflection angle β and contraction coefficient $C_c$ (8).

Until recently the complex nature of free jet and headbox flows precluded computer simulation. Headbox design was limited to educated guessing and physical modeling. The availability of robust and powerful codes to solve the Navier-Stokes Equations has made detailed flow simulation a possibility. Baliga and Mujumdar (9) summarize various numerical techniques for computing fluid flow in irregularly shaped domains such as the headbox. Uncertainty remains, however, as to the proper model for the structure of turbulence.

One particular package, FLUENT, based on the finite difference approach was chosen for this work. The turbulence intensity and eddy size were computed using the k-ε model defined originally by Launder and Spalding (10). The k-ε model contains four adjustable dimensionless constants which are assigned the default values in these studies (1). Model accuracy may vary from 10 to 50% depending on the nature of the problem (11).

## OBJECTIVES

The purposes of this work were to evaluate the effectiveness of computational fluid dynamics in predicting flow and turbulence characteristics and to better understand the effects of headbox design on the scale and intensity of turbulence. Three representative flow regimes were studied: the experimental straight-channel diffuser of D'Incau, an experimental Conver-flo headbox and a free jet issuing from the headbox.


1

Predictions from FLUENT are compared with experimental data for the straight-channel diffuser and the experimental headbox and against conformal mapping theory for the free jet.

## MODELING ASSUMPTIONS

The fluid was assumed to be Newtonian and fiber-free with viscosity of 1 cp. Turbulence was assumed to be isotropic and based on the standard k-ε model of Launder and Spalding. Inlet velocity and turbulence profiles were assumed to be constant in both directions normal to the flow (i.e., y and z). Walls are assumed to be perfect and the flow was computed on a uniform grid. Grid spacing differed for each application. Flow fields were two-dimensional in the headbox and free jet and three-dimensional in the straight channel.

Computations were made on a VAX11/780 minicomputer. Convergence of these two- and three-dimensional flows generally required from 500 to 1000 iterations.

## DISCUSSION

### Straight-Channel Diffuser

S. D.'Incau (4) measured turbulence intensity TI, macro length scale, ℓ, (an indication of eddy size) and turbulent strain rate, S, downstream of a rectangular grid placed in a straight channel as shown in Fig. 2.

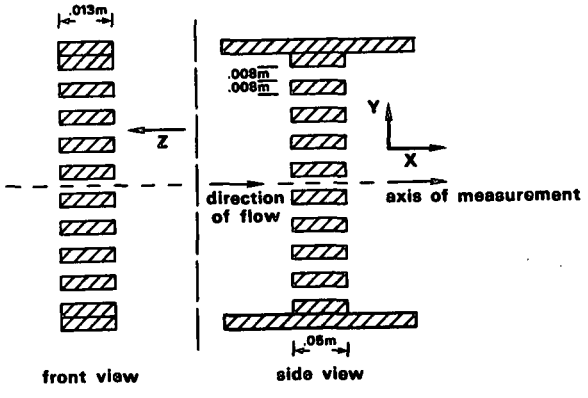


**Fig. 2** Geometry of the experimental straight-channel diffuser (4).

The grid consisted of 10 rectangular bars 0.008 m thick by 0.050 m long and 0.013 m wide spaced 0.008 m apart (d). Measurements were made along the centerline at eight locations downstream of the grid corresponding to z = x/d from 2 to 37.5 or from 0.016 to 0.3 m downstream. Average inlet velocity was 1.6 m/s. The Reynolds number based on channel width was 20000. Terms are defined in the nomenclature.

A uniform three dimensional grid 100x40x4 was used to define the flow. The grid points included the rectangular bars as well as the solid walls containing the flow. Turbulence intensity was assumed to be 10% at the entrance to the channel.

Turbulence intensity decayed in a first order fashion downstream of the grid as shown in Fig. 3. The decay was not affected by the presence of fibers at up to 0.45% consistency. The FLUENT predictions (fiber free) showed good agreement with the maximum value at the outlet of the grid and also with the rate of decay. However, the profile differs somewhat in shape and does not fall to as low a value. These results tend to support the validity of the k-ε model for turbulence for these types of flows. However, tuning of the turbulence parameters is obviously required for more precise fitting of the data.

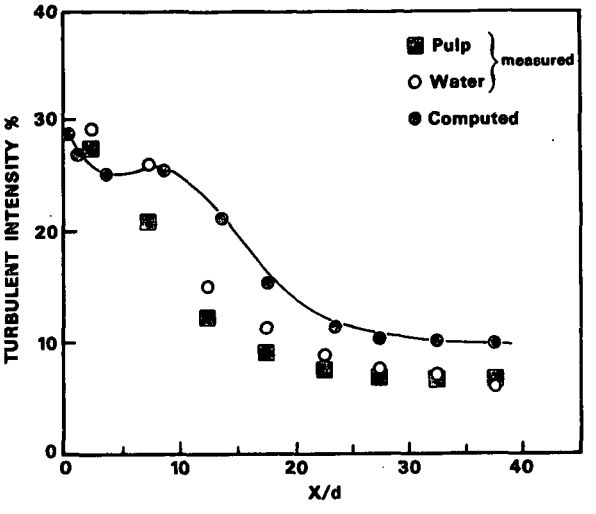


**Fig. 3** Turbulence intensity decay downstream of the grid in the straight channel diffuser.

Since typical turbulence intensity values entering and leaving the channel are on the order of 1 to 10%, the effect of the grid was to increase TI by a factor of 3 to 5 in the immediate neighborhood of the grid. TI decays back to its initial value at roughly 40 dimensionless lengths downstream.

Eddy size, ℓ, increased from a minimum value somewhat smaller than the diffuser slot height (0.008 m) immediately downstream of the grid to a scale comparable to the minimum channel dimension (0.015 m) as shown in Fig. 4. ℓ tended to remain constant for up to 8 diameters downstream before increasing. The FLUENT predictions showed instead a very constant value of the eddy size which was significantly smaller (0.00135 m vs. 0.005 m) than the measured values.

The reason for the constancy of ℓ predicted by FLUENT in this case was that the kinetic energy raised to the 1.5 power decreases at exactly the same rate as the decrease in dissipation rate, D. This is related to the relatively high value of TI far from the grid. High values of u' and TI result in high values of D which result in smaller ℓ. Adjustment of parameter $C_\mu$ in the k-ε model from 0.09 (default) to 0.3 failed to change this relationship. However, it did reduce KE and u' nearly uniformly throughout the flow field.

This result differed from other two-dimensional calculations in which the flow simply expands into a larger channel. These tended to show an increase in ℓ by a factor of 3 to 5 downstream of the expan-


2

sion in qualitative agreement with the measurements.

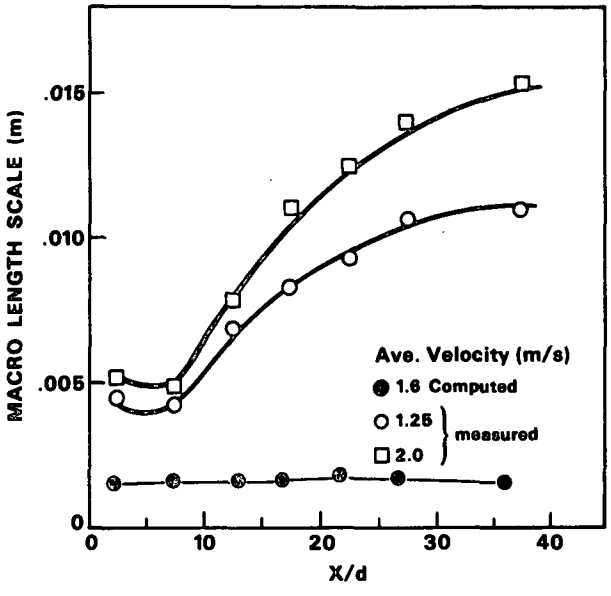


**Fig. 4** Eddy size variation downstream of the grid.

Fluctuating strain rate, S*, reached a maximum at approximately z = 7 as shown in Fig. 5. D'Incau also observed that maximum fiber dispersion occurred near z = 7.

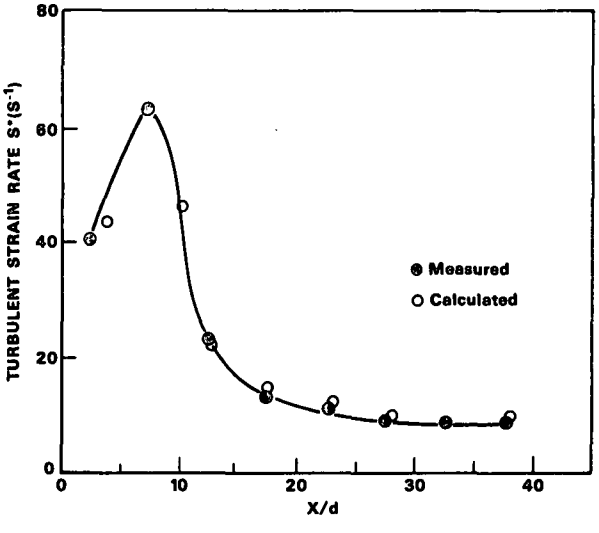


**Fig. 5** Measured and computed fluctuating strain rate profiles.

If the fluctuating strain rate is computed based on computed u' and measured ℓ, the computed values of S* agree quite well with the measurements, except for the absence of the maximum. This tends to add further validity to the k-ε model. The occurrence of the maximum indicates that either u' increases or ℓ decreases (or both) immediately downstream of the grid if the k-ε model is valid. Neither of these effects were observed for $C_\mu$ = 0.09. However, a distinct maximum was observed in KE and u' at approximately Z = 8 downstream of the grid for $C_\mu$ = 0.3. A slight maximum is observed for $C_\mu$ = 0.09. These differences could also result from experimental error or the location of the measurements.

Computed velocity contours downstream of the grid (Fig. 6) show regions of recirculating flow and stagnation points immediately upstream and downstream of the grid. They also show expansion of the jets downstream. Relatively uniform velocity and turbulence intensity are achieved at Z = 36 downstream of the grid where Z is based on the slot height.

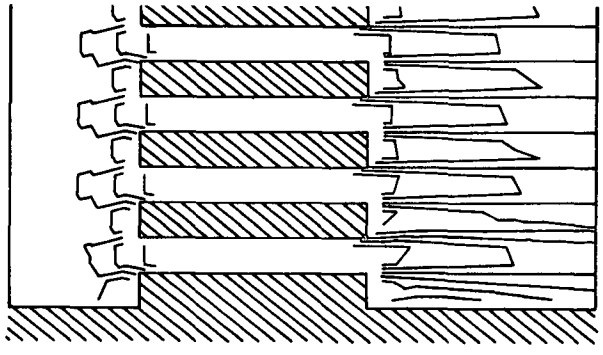

**Fig. 6** Computed velocity contour lines for the lower portion of the straight channel diffuser.

**Turbulence Generation in an Experimental Headbox**

The hydraulic headbox (12) creates high intensity turbulence but sometimes at the expense of increased jet instability and grainy formation resulting from small intense flocs. The relationship between eddy size and the minimum dimensions of the turbulence generator suggests smaller physical dimensions of the flow channels such as in Beloit's Thin Channel Conver-flo Hydraulic Headbox. A small scale experimental version shown in Fig. 7 was designed by Beloit to provide fundamental information about the effects of design and internals on turbulence levels.

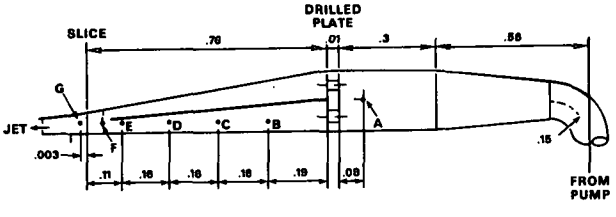


**Fig. 7** Side view of experimental Conver-flo headbox.

Several types of internals were evaluated. In case A the headbox contained a drilled plate containing eight holes as shown in Fig. 4. In case B 0.006 m ID tubes were added upstream of the drilled plate to provide a more uniform velocity distribution upstream of the plate. In case C the drilled plate was replaced by a slotted plate containing two rounded slots. The geometry of the internals are shown in Fig. 8.

Measurements of velocity, fluctuating velocity and turbulence intensity were made with the LDA tech-


3

nique at 7 locations along the x or machine direction in the lower channel as shown in Fig. 7 (13).

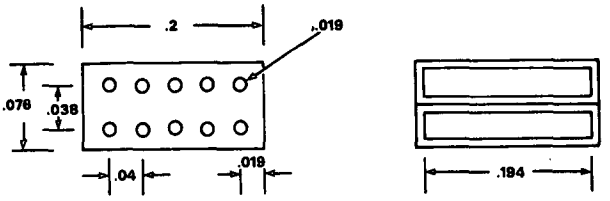


Fig. 8 Geometry of the drilled plate and slots used to generate turbulence.

Head box geometry was approximated by defining a uniform grid 100 x 60 in the x and y directions and by blocking out selected elements representing solid objects such as channel walls, splitter plate and the turbulence generator plate.

Cell dimensions ($\Delta x * \Delta y$) were 0.009144 m x 0.00127 m. Inlet conditions were specified at point A 0.0762 m upstream of the turbulence generator plate. Inlet velocity was 0.49 m/s in each case. Inlet turbulence intensity was assigned measured values of 42.7% for Case A and 22.9% for cases B and C, respectively.

Table 1 compares the measured and predicted values of average velocity and turbulence intensity for the three cases. Average velocity profiles were the same for each case so only values for case A are shown. Calculated velocity values differ significantly from measured values near the channel outlet (points F and G). This might be expected due to the relative coarseness of the grid near the outlet using the uniform grid. The differences were real since the measured values were reasonably close for all three cases. This indicates that the grid spacing can significantly affect the accuracy of the predictions. A cylindrical coordinate system or a variable grid would have been more appropriate for this type of flow. Body-fitted coordinates, which were not yet available, would also have solved this problem.

Table 1. Comparison of calculated and measured fluid flow data. Experimental Conver-flo headbox.

| | | | Turbulence Intensity, % | | | | | | |
|---|---|---|---|---|---|---|---|---|---|
| | Average Velocity | | Case A | | Case B | | Case C | | Predicted Eddy Length, m x $10^3$ |
| Location | Calc. | Meas. | Calc. | Meas. | Calc. | Meas. | Calc. | Meas. | |
| A | 0.49 | 0.49 | 37.8 | 37.8 | 19.6 | 19.6 | 19.6 | 19.6 | 2.7 |
| B | 0.71 | 0.70 | 12.9 | 36.2 | 12.3 | 36.5 | 8.1 | 11.1 | 3.6 |
| C | 0.84 | -- | 7.1 | 12.4 | 7.0 | -- | 5.3 | -- | 3.4 |
| D | 1.16 | -- | 4.0 | 6.1 | 4.0 | -- | 3.3 | -- | 1.9 |
| E | 2.45 | 2.64 | 2.5 | 2.4 | 2.5 | 2.4 | 2.4 | 2.7 | 0.3 |
| F | 2.90 | 3.50 | 8.8 | 1.8 | 10.6 | 1.9 | 8.5 | 1.7 | 0.7 |
| G | 4.91 | 6.51 | 4.6 | 1.3 | 4.6 | 1.4 | 4.8 | 1.3 | 0.5 |

The tubes upstream of the plate significantly reduced TI entering the channels for Cases B and C. Turbulence intensity tended to decrease exponentially downstream, in general agreement with previous results. In Case A, however, TI levels did not drop until after point B while FLUENT predicted a continual decrease. TI dropped off more rapidly for the slotted plate (Case C) than for the drilled plate due to the higher flow area and reduced shear intensity.

As with the velocity, predicted TI at points F and G were less accurate due to the relative coarsening of the grid as the channel height decreased.

Predicted eddy length shown in the table decreased significantly along the channel due to the continual decrease in channel height in the Conver-flo design.

The computations provide a nearly continuous profile, while experimental results may miss significant details due to the placement of the measuring device. For example, the TI profile for Box A shows a local maximum at about 7 diameters downstream of the plate. (z = 7) downstream of the drilled holes as shown in Fig. 9. Eddy size also shows a local maximum of 0.004 m at z = 12.

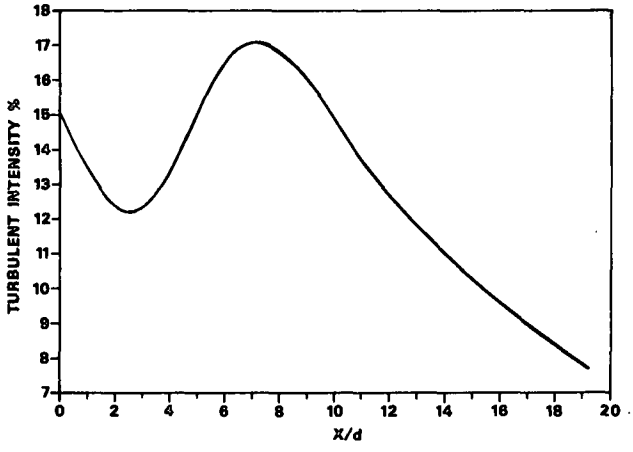


Fig. 9 Turbulence intensity profile for the Conver-flo headbox Case A.

Streamline contours for Case A in Fig. 10 show recirculation zones and boundary layer reattachment at about z = 7.

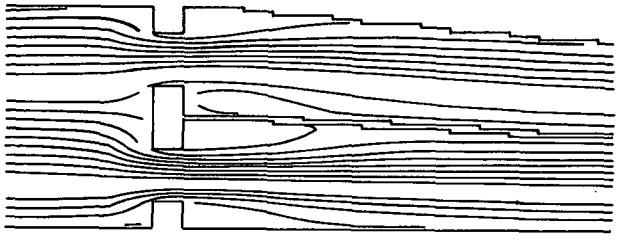

Fig. 10 Contour lines for the experimental headbox.

**Free Jet Flow and Geometry**

The jet angle determines initial forming conditions and thereby affects formation and other qualities of the sheet. The contraction coefficient determines the effective headbox consistency and flow out of the box at a given speed. The jet's turbulent kinetic energy and average velocity profile may be indicative of the stability and streaking tendency of the jet. Vortices can be formed due to the change of direction of the flow around the slice lip hangdown. Predicting the velocity profile in this region may be helpful in understanding and quite possibly predicting these phenomena.

For the free jet we compare the predicted jet exit angle, contraction coefficient, turbulent kinetic energy profile and average velocity profile with the analytical solutions valid for irrotational flow (TAPPI charts, Fig. 1).

For the computation the slip boundary condition was specified along the free surfaces of the jet. A uniform inlet velocity of 0.49 m/s was assumed based on the measured volumetric flow rate into the headbox. Velocity does not, however, affect the geometry of the jet in irrotational flow nor does it enter into the predicted jet angle and contraction coefficient in the TAPPI curves. Computations were based on a uniform two-dimensional grid.

The free surface geometry was determined by trial and error adjustment of the angles of the "walls" until the $\varepsilon$ (i.e., free surfaces) were approximately atmospheric. In this case, the TAPPI curves provided values of the jet angle and contraction coefficient. From these the initial free surface boundary was estimated. Predicted streamlines were parallel to the jet boundaries, and boundary pressures were approximately atmospheric, indicating that no further adjustments were required.

To test the sensitivity of the jet geometry, an incorrect jet angle and contraction coefficient were used. The resulting stream lines intersected the surfaces of the jet and the surface pressures were not atmospheric. This indicated that had a trial and error approach been used from incorrect starting boundaries, FLUENT would have eventually predicted the jet shape in agreement with theory.

Figure 11 shows the streamlines predicted by FLUENT with the boundary shape guessed from the TAPPI curves using the following geometrical parameters: $L/b = 0, \alpha = 45$ degrees, and $b/B = 0.5$. Theoretical values of jet angle ($\beta$) and contraction coefficient are = 14.8 degrees and 0.83, respectively. The consistent agreement between the FLUENT and TAPPI jet shapes and streamline profiles indicates that the assumption of irrotational flow in the jet is obviously justified. This may not be valid for high consistency forming conditions, however. It also shows that free jet flows can be computed accurately.

The turbulent kinetic energy contours shown in Fig. 12 indicate that significant increases in turbulence occur at the slice. This provides quantitative evidence of the important role played by slice geometry in floc breakup. However, in practice, it may be difficult to predict the effect of small but important angle changes on jet shape because of the difficulty in differentiating the pressure and streamline variations.

## CONCLUSIONS

These results show that computational fluid dynamics can provide a significant predictive tool in headbox design. The k-$\varepsilon$ model appears to predict turbulence behavior reasonably well for these geometries. Some tuning of the k-$\varepsilon$ parameters may be required for each situation. This requires that some experimental data be available to provide a basis for tuning the parameters. The only reservation is in the predicted eddy size variation.

Although in the particular case shown, $\ell$ remained constant, other flow cases showed an increase in agreement with measurements.

**b/B = 0.5**
**$\alpha$ = 45°**
**L/b = 0**
**Jet Angle (Theoretical)= 14.8°**
**Contraction Coefficient = 0.83**

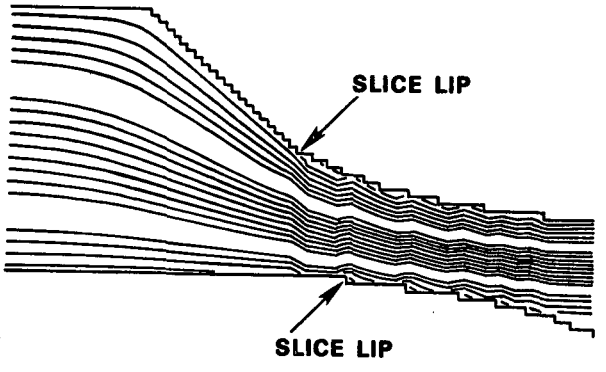


**Fig. 11** Streamline contours and jet shape predicted by FLUENT.

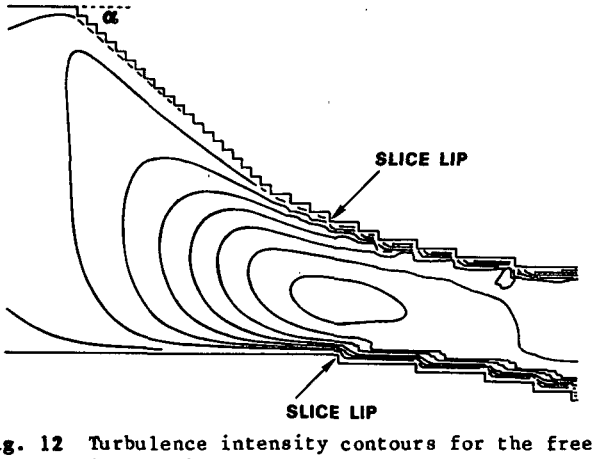


**Fig. 12** Turbulence intensity contours for the free jet predicted by FLUENT.

Turbulence intensity and scale are strongly dependent on the scale of the grid generator and on the Reynolds Number based on the grid scale. Both intensity and strain rate decay exponentially downstream. Eddy size increases in a first order fashion downstream.

Accurate predictions of flow and turbulence profiles are highly dependent on choice of the appropriate coordinate system and grid spacing. Much needs to be done in the area of modeling floc formation "kinetics" in flow fields in order to extend the predictions to the multiphase fiber flow system. Also much remains to be learned about how to generate and control turbulence scale and intensity.

## ACKNOWLEDGMENTS

Portions of this work were used by R. J. Ginnow as


5

partial fulfillment of the requirements for the Master of Science degree at The Institute of Paper Chemistry. The authors wish to thank member companies of The Institute of Paper Chemistry and their affiliates for their generous support of this research. Special thanks go to Dr. Jay Shands and Beloit Corporation for providing the experimental data of the pilot headbox.

**NOMENCLATURE**

TI turbulence intensity % = u'/uavg * 100.

S turbulent strain rate (1/s) = u'/(2*ℓ).

uavg x-direction average velocity (m/s).

u' time-averaged x-direction velocity fluctuation (m/s)

ℓ eddy size ($10^{-3}$m) = $C_u^{3/4}KE^{3/2}/D$ where $C_u$ = 0.09.

D = dissipation function = ε in the k-ε model ($m^2/s^3$).

KE = turbulent kinetic energy = 3 $u'^2/2$ = k in the k-ε model ($m^2/s^2$).

**REFERENCES**

1. FLUENT MANUAL, Creare Incorporated, Hanover, New Hampshire, (June, 1985).

2. Smook, G. A., Handbook for Pulp and Paper Technologies, Joint Textbook Committee of the Paper Industry, TAPPI/CPPA, McGraw-Hill, (1982).

3. Mason, S. G., Pulp Paper Mag. Can. 49(13): 99-104 (1948).

4. D'Incau, S., TAPPI Proceedings, 1983 Engineering Conference, 1983: 583-92.

5. Chuang, S. C., 1982 TAPPI Engineering Conference, Fluid Mech. Session, San Francisco, Sept. 13-16 (1982).

6. Bercel, E., E. Shuffler, Pulp Paper Mag. Can. 82(6): T221-4 (1981).

7. Appel, D. W., Y. S. Yu. "Free Streamline Analysis of Flow from Nozzle, Flow Through Side Inlets and Flow Past Corners," University of Kansas, Studies in Engineering Mechanics, Report No. 17 (1963).

8. TAPPI Technical Information Series TIS 014-2, 3,4.

9. Baliga, B. R., A. S. Mujumdar. "On the Numerical Prediction of Confined Flows in Irregular-Shaped Domains." Proc. Intern. Symp. Paper Machine Headboxes, 74-83 (1979).

10. Launder, B. E., D. B. Spalding. Mathematical Models of Turbulence, Academic Press, London, (1972).

11. Launder, B. E., A. Morse. Turbulent Shear Flows, p. 279-294, Springer-Verlag, Berlin, (1979).

12. Waller, M. H., Tappi J. 33-41 (Jan., 1987).

13. Shands, J., Beloit Corporation, private communication (1987).



6

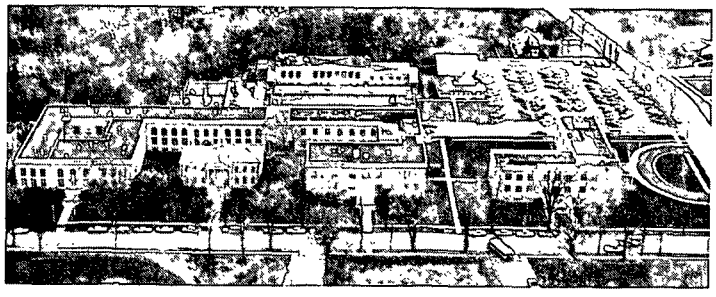

THE INSTITUTE OF PAPER CHEMISTRY, APPLETON, WISCONSIN

IPC TECHNICAL PAPER SERIES
NUMBER 292

# A COMPARISON OF COMPUTATIONAL AND EXPERIMENTAL METHODS FOR DETERMINING THE GAS FLOW PATTERNS IN THE KRAFT RECOVERY BOILER

A. K. JONES, T. M. GRACE, AND T. E. MONACELLI

JUNE, 1988

# A Comparison of Computational and Experimental Methods for Determining the Gas Flow Patterns in the Kraft Recovery Boiler

A. K. Jones, T. M. Grace, and J. E. Monacelli

Portions of this work were used by AKJ as partial fulfillment of the requirements for the Ph.D. degree at The Institute of Paper Chemistry. This is to be presented at the TAPPI Engineering Conference in Chicago on September 19-22, 1988

# A COMPARISON OF COMPUTATIONAL AND EXPERIMENTAL METHODS FOR DETERMINING THE GAS FLOW PATTERNS IN THE KRAFT RECOVERY BOILER

A. K. Jones and T. M. Grace
The Institute of Paper Chemistry
Appleton, WI 54912

J. E. Monacelli
Babcock & Wilcox
Power Generation Group
Barberton, Ohio 44203

## ABSTRACT

Computational fluid dynamics was applied to the problem of gas flow in a kraft recovery furnace. For simplicity, the case chosen to be modeled is the "cold flow case" (the gas flow pattern that derives directly from the method of air introduction and furnace geometry, without complications from combustion, temperature distributions, and liquor spray interactions). The framework for the computational model was FLUENT (a commercially available, finite difference, computational fluid flow program). A three-dimensional description of the recovery furnace with 50,000 computational cells was used. Bilateral symmetry of the furnace was assumed to reduce the computational effort by a factor of two. The results of the computational model are compared with experimental cold flow data obtained on a 1/8th scale model of a recovery furnace. The analytical model corresponded closely with the experimental cold flow data.

## INTRODUCTION

This paper describes the first stage in the development of a three-dimensional recovery furnace model, namely, the simulation of cold flow in an existing furnace design. In a cold flow model only the geometry and method of introduction of the air are assumed to be important. Neglected are the effects of temperature, combustion, and in this case the interaction between the black liquor spray and the gas phase. A particular B&W furnace, located in DeRidder, LA, was simulated, as data were available for comparison (1). B&W measured the velocity profiles in a 1/8th scale replica of this furnace design, under a number of flow conditions. This paper examines two computationally developed flow patterns in this recovery furnace, obtained by using FLUENT (a commercially available computational fluid flow program), and compares them with two experimentally determined flow patterns.

The computational flow field is found by use of an analytical cold flow model of the DeRidder unit at 273K. The experimental flow field was developed in a 1/8th scale model of this same recovery furnace. The B&W report then provides scaling constants for converting the velocities up to the full sized furnace at 477K. These velocities are then corrected to 273K in order to make a comparison to the computational work.

## A DESCRIPTION OF FLUENT

The main tool used in the computational simulation was FLUENT, a finite difference program for the modeling of fluid flows. FLUENT is flexible and comprehensive, permitting its use in a wide variety of flow situations, including two or three dimensional flows, laminar or turbulent flows, and swirling flows. Additional features of FLUENT include a six-flux radiation model, the PSI-CELL model for two-phase flow (2), a combustion model, a number of turbulence models, and a porous flow model.

The variables that are solved for in the simplest three-dimensional case are u-velocity, v-velocity, w-velocity and pressure. If temperature effects are added, the enthalpy and the radiative heat fluxes are also determined. If the K-turbulence model is used, then the kinetic energy of turbulence and the dissipation rate are found. If combustion is included, the mole fractions of combustibles (F), oxygen (O), and products (C), must be calculated in each cell. The maximum number of finite element cells that can be solved for in the version of FLUENT used (version 2.8) is 50,000.

The attractive features of FLUENT are 1. interactive input; 2. flexibility - almost any type of flow can be modeled; 3. internally generated relaxation coefficients, which usually result in stable iterations; and 4. excellent graphics for viewing the results.

The process of setting up a fluid flow simulation is straightforward, as the description of a flow is menu driven. Cartesian or cylindrical regions can be described. In a cartesian description the cells are rectangular parallelpipeds that can be different lengths in each coordinate direction. A number of different cell types can be specified. Typically five different types are used: 1. live cells - the variables in these cells are solved for at each iteration; 2. inlet cells - the values of the flow variables are specified for these cells and remain the same throughout the calculation; 3. wall cells - these cells act as barriers to the flow and are used to describe the flow geometry; 4. outlet cells - the value of the flow variables are solved for, but these cells are placed on boundaries of the flow; 5. symmetry cells - they define lines or planes of symmetry in the flow, which reduces the number of cells necessary to describe a given flow geometry.

In addition to a description of the flow geometry, it is necessary to specify the physical properties of the fluid and the boundary conditions in the wall and inlet cells. The mass flow rates in the inlet cells are controlled by varying the gas velocity or the distance between adjacent nodes.

## THE COLD FLOW SIMULATION

The analytical "cold flow" model was set up with physical dimensions as close as possible to those of the full-sized furnace, in order to justify comparison between the experimental and analytical cases. The upper limit of 50,000 nodes makes it



1

necessary to use some approximations. An isoparametric view of the furnace is shown in Fig. 1 and 2. Due to the symmetry involved, it is only necessary to describe half of the furnace. The flow patterns in the other half of the furnace will be a mirror image of the area of the furnace modeled. The symmetry plane is parallel to the side walls and cuts the bullnose and bed in half.

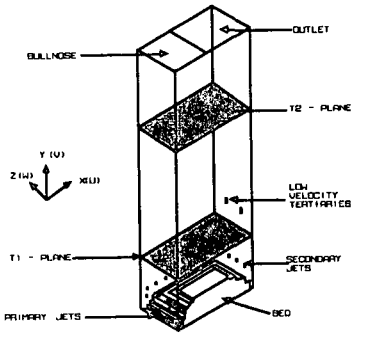


**Fig. 1** Illustration of furnace geometry low velocity tertiaries.

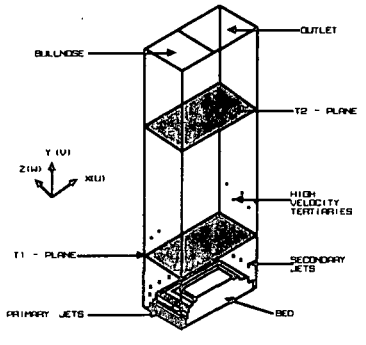


**Fig. 2** Illustration of furnace geometry high velocity tertiaries.

The full-sized furnace is 9.6 meters by 10.6 meters in cross section and 27.0 meters high (to the bullnose). The FLUENT model is 10.0 meters by 5.0 meters (due to symmetry) and 30.0 meters high. The bullnose extends 5 meters across the top of the furnace in both cases. The bullnose slopes slightly downward to the back of the furnace, but this was ignored in the computational model in order to reduce the number of nodes used. The resulting effect on the gas flow patterns should be negligible, as the slope is minimal.

The air inlets were modeled in the following manner:

**Primary Air**

A row of nodes along the walls were designated as inlets; the distance between the inlet nodes and the nodes above and below were adjusted in order to satisfy the volumetric flow rates. This treats the primary air as if it was a planar jet completely encircling the furnace. A shortage of nodes made description of individual primary ports impractical. The primary air was injected 1 meter above the furnace floor at a velocity of 40 meters/sec.

**Secondary Air**

Individual air ports of approximately the same dimensions as the ports in the actual furnace were used for the secondary air. The dimensions of the ports in the full-sized furnace were 7.6 cm by 35.5 cm. In the model they were 11.4 cm by 23.7 cm. The areas were the same; the individual dimensions had to be adjusted. This approximation was necessary due to computer hardware limitations that restricted the total number of cells that could be used. The width of the secondary and tertiary air ports (11.4 cm) was an average of the actual widths. The half of the furnace modeled had 16 secondary ports, each with an inlet velocity of 36 meters/sec (identical to the prototype furnace). The injection level was 3 meters above the furnace floor.

**Tertiary Air**

Separate air ports on the walls were used, with approximately the same shape as those in the actual furnace. Two configurations were examined. In the first configuration 4 ports at 10 meters above the furnace floor were used, two on each the front and back walls, with an inlet velocity of 10 meters/sec, (identical to the prototype furnace), as shown in Fig. 3. The port sizes were 11.4 cm by 1.02 m, the same area as the actual ports which were 15.2 cm by 76.2 cm. In the second configuration, 8 smaller ports with an inlet velocity of 77 meters/sec were used, four on each the front and back walls. Two closely spaced levels of tertiary air were used (at 9.5 and 10.5 meters above the floor of the furnace), this is shown in Fig. 4. The port sizes in this case were 11.4 cm square, as opposed to the 12.7 cm ID circular ports used in the actual furnace.

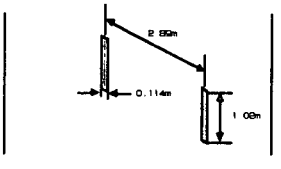


**Fig. 3** Low velocity tertiaries.

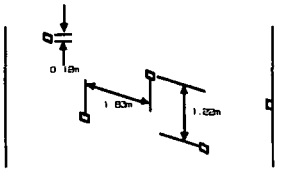


**Fig. 4** High velocity tertiaries.

Two computational cases were examined: the first corresponds to experimental case 1, with the low velocity tertiaries; the second to experimental case 2, with the high velocity tertiaries. The computational cases were set up so that they corresponded as closely as possible to the two experimental cases.


2

The bed shape used (Fig. 5) corresponded as closely as possible to the one used in the experimental work (Fig. 6); with the top of the bed extended slightly above the secondary air ports. The use of body fitted coordinates would eliminate the staggered bed shape and the resulting numerical problems, leading to a more accurate description of the flow around the bed, but this is not yet available as part of FLUENT.

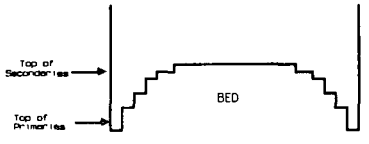


**Fig. 5** Outline of computational bed model.

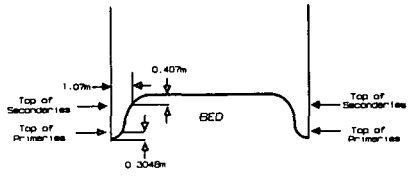


**Fig. 6** Dimensions of experimental bed model.

The mass flow rates in the FLUENT models were the same as the full-sized B&W furnace; the total flow rate for the half of the furnace modeled was 48 kg/sec (380,000 lb/hr). In case 1 the flow was split into 50% primary, 40% secondary and 10% tertiary air. In case 2 the flow was split into 46% primary, 36% secondary and 18% tertiary air.

## EXPERIMENTAL DATA

The experimental data used for comparison with the analytical cold flow models were part of a B&W investigation (1). The furnace examined was the Boise Cascade Process Recovery Boiler, located in DeRidder, LA. This furnace was experiencing excessive particulate carryover. The problem was believed to be due to insufficient breakup of a high velocity core of gas by the existing tertiary air jets.

A number of changes in the tertiary air system were considered. These changes were evaluated by constructing a 1/8th scale replica of the DeRidder recovery furnace, and conducting cold flow measurements in this replica. The velocities within the scaled-down furnace were measured with a hot film anemometer at two traverse planes, T1 located halfway between the secondary and tertiary air ports, and T2 located about halfway between the tertiary air ports and the bullnose. Isovelocity plots were constructed using these data.

The two cases that were simulated will be designated case 1 and case 2. In both cases a bed was included in the bottom of the furnace; the shape of this bed is shown in Fig. 6.

## RESULTS - A COMPARISON BETWEEN THE EXPERIMENTAL AND COMPUTATIONAL CASES

This section will describe in detail the results of modeling with FLUENT the two cases described earlier and compare these results with the experimental cases. The contour plots will be compared on the basis of average upward velocity at 273K, and on the general flow pattern.

In order to make a comparison of the experimental and computational cases it is first necessary to put them on an equal basis. In the experimental work the average upward velocity is calculated by adding together all the positive velocities and dividing by the number of these positive velocities. The average upward velocity in the prototype (full-size furnace at 400°F) can then be calculated based on scaling criteria. In case 1 the scaling factor is 218, in case 2 it is 295. This results in an average velocity in feet/min which can then be converted to m/sec. Finally, a temperature correction is applied converting the experimental results to 273K. The results obtained computationally are already in m/sec, at the cold flow temperature of 273K.

### Case 1 - T1 Traverse

The T1 traverse is a horizontal slice located above the bed as shown in Fig. 1. Contours of the upward velocity (V-velocity) are shown in Fig. 7 and 8 (experimental and computational results).

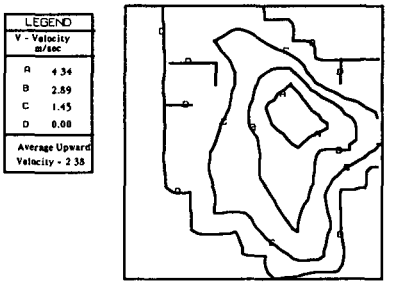


**Fig. 7** Low velocity tertiaries - T1 slice experimental results.

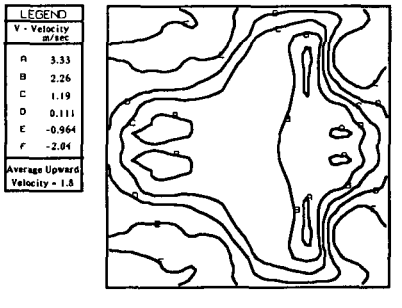


**Fig. 8** Low velocity tertiaries - T1 slice.

The main features of these contour plots are the upflow region in the center of the furnace and the downflow regions around the outside. The computational T1 traverse for case 1 shows good agreement with the experimental results with respect to the general flow patterns, with the location of downflow regions and the maximum upward velocity corresponding to the experimental results. The average upward velocity is about 40% higher in the experimental case than in the computational case (2.40 m/sec vs. 1.80 m/sec). This is due to the use of a staggered bed; the air jets tend to be


3

deflected upward rather than following the surface of the bed. This reduces the intensity of the central core, as some of the gas is deflected upward before it reaches the center of the furnace.

The velocities are highest in the center as all the secondary jets meet at this point and are forced to move upward. The downflow regions around the perimeter of the furnace are created due to entrainment of gas by the secondary jets.

**Case 1 - T2 Traverse**

At the T2 traverse, a horizontal slice located above the tertiary jets (see Fig. 1), the velocity contours obtained experimentally have taken on a much different appearance. This is shown in Fig. 9. At the back of the furnace a region of recirculation is present. At the front of the furnace the upward velocities are large. The back of the furnace is a large stagnant region, resulting in poor use of the furnace volume for combustion of the flue gases.

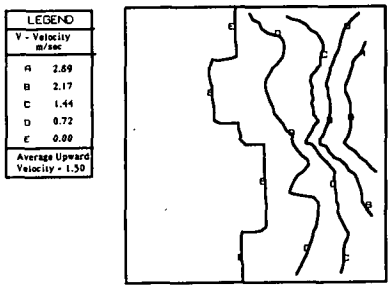


**Fig. 9** Low velocity tertiaries - T2 slice experimental results.

At the T2 traverse in case 1 the existence of a large stagnant region seen experimentally is confirmed using FLUENT (Fig. 10). The location of the maximum upward velocity is at the front wall in both cases. The average upward velocity in the experimental case is 1.50 m/sec, compared to 0.83 m/sec in the computational case. This is once again a result of the numerical problems discussed earlier, persisting up to the T2 traverse.

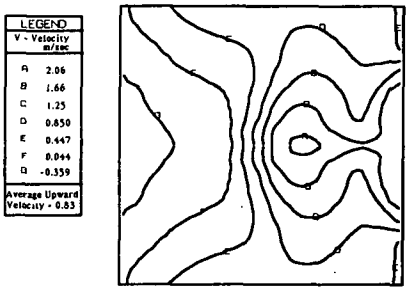


**Fig. 10** Low velocity tertiaries - T2 slice.

**Case 2 - T1 Traverse**

The comparison at the T1 traverse for case 2 is essentially the same as for case 1, except that the discrepancy in the average upward velocity is higher (1.60 vs. 2.94 m/sec) (Fig. 11 and 12).

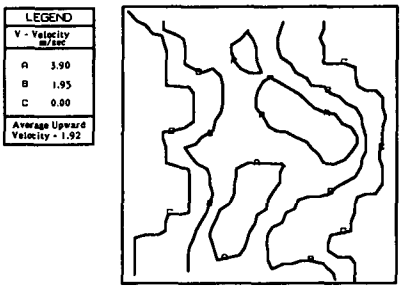


**Fig. 11** High velocity tertiaries - T1 slice experimental results.

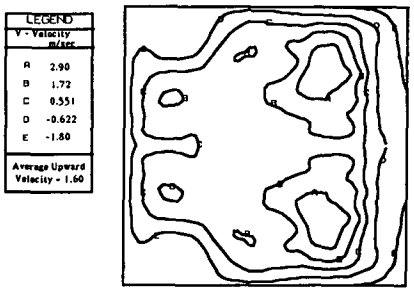


**Fig. 12** High velocity tertiaries - T1 slice.

**Case 2 - T2 Traverse**

Case 2 has much higher velocity tertiaries; this results in a better utilization of the furnace volume, as shown in Fig. 13. The stagnant region at the back of the furnace has been eliminated.

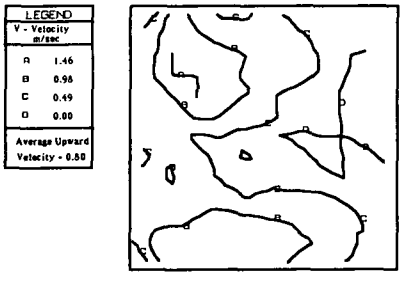


**Fig. 13** High velocity tertiaries - T2 slice experimental results.

The experimental T2 traverse in case 2 has no downflow; the computational results have only small areas of downflow against the side walls (Fig. 14). The average upward velocity found experimentally and computationally are both 0.80 m/sec. The numerical problems are no longer a factor as the center core has been almost completely eliminated in both cases, and the average upward velocity should be just the total mass flow rate divided by the cross sectional area times the density; which is the same in both cases.

The reason for the elimination of the stagnant region can be seen by comparing Fig. 15 and 16. Contours of the U-velocities are shown on a horizontal slice that cuts through the midpoint of the tertiary jets. Immediately apparent is the difference in penetration distance between the two


4

cases. This increased penetration allows breakup of the core of high velocity gas created in the lower furnace.

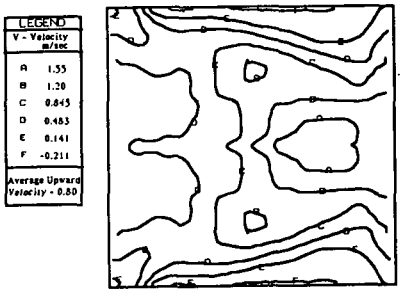


**Fig. 14** High velocity tertiaries - T2 slice.

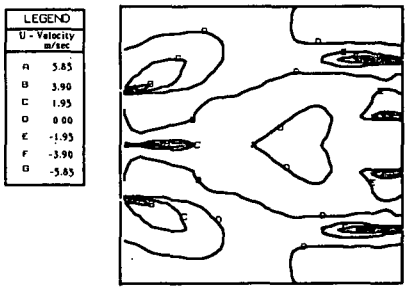


**Fig. 15** Low velocity tertiaries - tertiary jets.

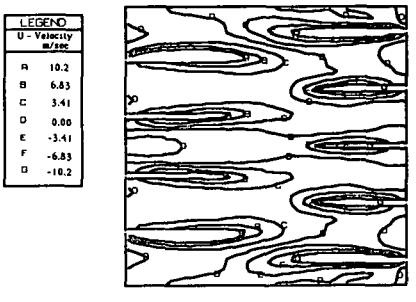


**Fig. 16** High velocity tertiaries - tertiary jets.

## LIMITATIONS OF MODELING TECHNIQUES

Both numerical and experimental scale modeling have inherent drawbacks. Both can be effective if the limitations of these techniques are kept in mind.

The main limitations of computational modeling are 1. the need to use staggered nodes to describe a diagonal surface (i.e., bed surface); 2. the empiricism of built-in turbulence models; 3. the large amount of computer time required to converge complex problems, (a typical problem takes about 7 days of CPU time to converge on a MicroVax); 4. the difficulty in deciding when a flow pattern has converged; and 5. the limitation in the number of nodes, making it impossible to describe fine details of the flow around the bed and in jets.

Experimental scale modeling of gas flows has the following limitations: 1. once a scale model has been constructed, only minor changes can be made in the geometry; 2. it is difficult or impossible to satisfy all the scaling criteria; 3. it is very difficult to measure large numbers of velocities within the model, and these velocities may be altered by the act of measuring them; 4. temperature effect cannot be easily added.

## CONCLUSIONS

The main conclusions that can be drawn from the modeling effort thus far are

1. FLUENT can be used effectively to simulate the flow patterns in the kraft recovery boiler;

2. The benefit of modifying the tertiary jets in the B&W furnace can be observed by the use of FLUENT, in agreement with experimental results;

3. Numerical problems are created due to the primary and secondary air jets impacting on the staggered bed. In future modeling work the bed will not extend above the level of the secondaries. This should result in a more realistic flow pattern.

## ACKNOWLEDGMENTS

Portions of this work were used by AKJ as partial fulfillment of the requirements for the Ph.D. degree at The Institute of Paper Chemistry.

## LITERATURE CITED

1. Dykshoorn, P. Process Recovery Boiler Flow Model Tests, RDD:87:6940-01-01:01, July, 1986.

2. Crowe, C. T. and Sharma, M. P. The Particle-Source-In-Cell (PSI-CELL) Model for Gas-Droplet Flows. Journal of Fluids Engineering, 99:325-32 (July 1977).



5